EDGE ARTICLE

Check for updates

Glutathione-activatable synthetic channel for hopping-mediated anion transport

Sandip Chattopadhayay, [ID] [a] Debraj Ganguly, [a] Triveni Sodnawar [b] and Pinaki Talukdar [ID] *[ac]

Controlled transport of ions across the cellular membrane is an essential process. While nature employs stimuli-gated transmembrane proteins to facilitate the appropriate transport of essential ions or molecules across cellular membranes, the endeavor to create a stimuli-controlled synthetic analogue presents considerable challenges. Herein, we introduced isophthalamide-based synthetic ion transporters **1a–1e** and a protransporter **1c′**. Transport studies divulged that even though the protransporter **1c′** cannot transport the anions, the glutathione-based activation generates a self-assembled anion channel **1c** in the membrane and turns ON the anion transport with preferential selectivity towards the chloride anion. Detailed mechanistic studies validated that the transport of anions occurs *via* the antiport mechanism. An electrophysiological experiment divulged that the protransporter is inefficient in forming stable channels in the membrane. In contrast, the addition of the GSH releases the compound **1c**, which forms a stable channel in the membrane with an average diameter of 4.7 ± 0.3 Å. The calculated single-channel conductance is 165 ± 1 pS, and the average $P_{Cl^-}/P_{K^+} = 5.0 \pm 1.3$. A dodecameric assembly of the monomeric rosette of **1c** and $[(\mathbf{1c})_{12} + Cl^-]$ was geometrically optimized to understand the ion channel formation and investigate the responsible channel–ion interactions for the ion transport process.

1 Introduction

The cellular membrane acts as a protective layer, preventing unwanted guests from entering while allowing the selective passage of ions or large polar molecules to maintain normal physiological functions.[1–3] Membrane-embedded, structurally and functionally complex proteins, such as ion channels and pores, control ion translocation in response to specific stimuli. Importantly, malfunctions in these transmembrane proteins can result in serious diseases known as channelopathies.[4–6] Consequently, the design of synthetic transporters offers promising prospects. These synthetic channel-forming molecules hold potential applications in elucidating transport mechanisms, advancing drug delivery systems, developing biosensors, and providing therapeutic solutions for various channel-related diseases.

Inspired by nature, different stimuli-gated systems have been developed in recent years to modulate the movement of the ions across the bilayer membrane. Different stimuli have

been used to control the ion transport process across the membrane, including pH, light, ligands, voltage, enzymes, and GSH.[7–18] With the parallel development of pH, light, enzyme, and ligand-gated synthetic transporters in recent years, designing a synthetic transport system in which the ion flux can be modulated with GSH also requires significant attention. GSH as a stimulus in synthetic ionophore systems creates hope for generating an alternative strategy to decorate different stimuli-gated synthetic ion transport systems, thereby opening up avenues for their utilization in various therapeutic applications.

The GSH-mediated transport activation concept was introduced by Manna and coworkers using synthetic transporters.[18] A GSH-triggered activation was used in thiourea-based tripodal compounds to activate the Cl⁻ ion transport process. Gabbaï and coworkers introduced GSH as an external stimulus for controlling the Cl⁻ ion transport activity of antimony-based anion transporters by manipulating both the lipophilicity of the transporter and its overall anion affinity.[14] Gale and associates invented gold complexes as efficient switchable anion transporters by complexing bisimidazole anion transporters with Au^{III}, which blocks the anion binding site.[19] A GSH-based decomplexation of gold initiates the H⁺/Cl⁻ cotransport by releasing the active transporter across the liposome. Recently, Manna and coworkers developed a thiourea-based procarrier linked with the Arg–Gly–Asp (RGD) peptide.[20] The GSH-induced release of active transporter from the procarrier initiated H⁺/Cl⁻

[a] Department of Chemistry, Indian Institute of Science Education and Research Pune, Dr Homi Bhabha Road, Pashan, Pune 411008, Maharashtra, India. E-mail: ptalukdar@iiserpune.ac.in

[b] Department of Biotechnology, Savitribai Phule Pune University, Pune 411007, Maharashtra, India

[c] Department of Chemistry, School of Natural Sciences, Shiv Nadar Institution of Eminence, Delhi NCR 201314, India
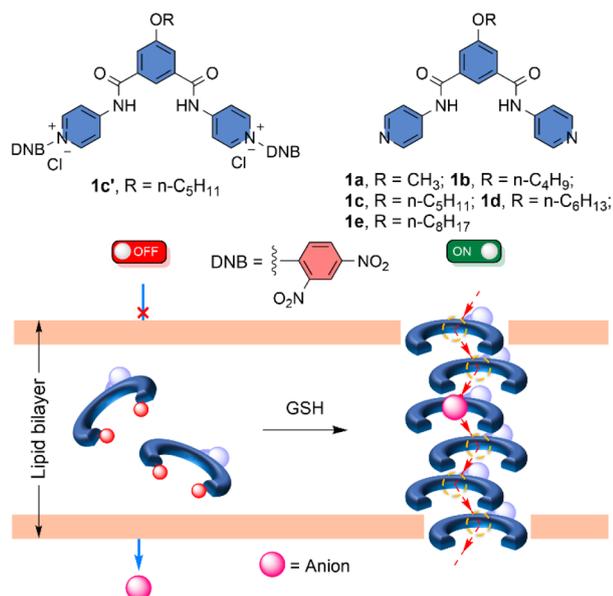
Fig. 1 Chemical structure of compounds **1a–1e** and **1c′**, and graphical representation of the generation of barrel-rosette anion channel from the corresponding protransporter by using GSH as a stimulus.

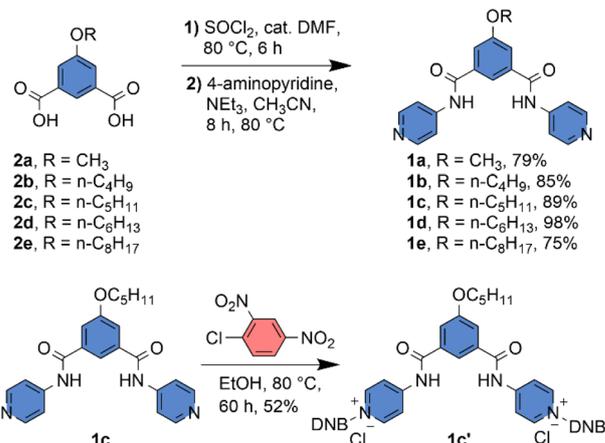**Scheme 1** Synthetic scheme of compounds **1a–1e** and **1c′**.

cotransport. All of the above-mentioned examples are based on synthetic carrier systems. In the domain of artificial ion channels, our group developed the GSH-triggerable ion channel system for the transmembrane transport of cation–anion pairs.[12] The rare example of a GSH-based activation in the synthetic ion channel continuously stimulates our intellectual pursuit to introduce different synthetic ion channels where GSH can trigger ion transport activity.

Herein, we designed an isophthalamide-based self-assembled barrel rosette ion channel **1a–1e**, which can transport the anion across the membrane (Fig. 1). Different synthetic analogues were used to modulate the membrane insertion efficiency by altering the lipophilicity of the channel-forming molecule. Moreover, to mask the ion transport activity, the pyridine groups of compound **1c** were attached to the 2,4-dinitrochlorobenzene (DNCB) to generate the protransporter **1c′**. The attachment of 2,4-dinitrobenzene (DNB) to the transport active channel molecule decreases membrane insertion efficiency by altering lipophilicity and disrupting the self-assembly process. Therefore, it is expected that no transport behaviour will be shown across the membrane. Notably, the addition of GSH can turn ON the transport process by releasing the channel-forming molecule in the membrane,[21] which can self-assemble to form the barrel-rosette anion channel.

2 Results and discussion

2.1 Design and synthesis of 1a–1e and 1c′

Compounds **2a–2e** were synthesized as described in the SI. Compounds **2a–2e** were treated with $SOCl_2$ with catalytic DMF at 80 °C to convert them to the corresponding acid chloride. The acid chloride was directly coupled with 4-aminopyridine at

80 °C with NEt_3 as a base and CH_3CN as a solvent to obtain the desired compounds **1a–1e** with a significant yield (Scheme 1). The protransporter **1c′** was synthesized by reacting **1c** with 2,4-dinitrochlorobenzene at 80 °C in EtOH solvent (Scheme 1). All compound characterization data are provided in the SI.

2.2 Self-assembly and morphological study

The self-aggregation property of compound **1c** was initially investigated with concentration-dependent ^1H NMR in $CDCl_3$ solvent at 25 °C. Increasing the concentration of compound **1c** also increased the downfield shift of the H_a proton, indicating that at elevated concentrations, the compound is capable of forming intermolecular H-bonding (Fig. S2). Furthermore, the temperature-dependent ^1H NMR experiment confirmed that increasing the temperature results in an upfield shift of the H_a proton (Fig. S3). This data revealed that an elevation in temperature breaks the intermolecular H-bonding, thereby upfielding the H_a proton. Furthermore, to understand the aggregation pattern of compound **1c**, field-emission scanning electron microscopy (FESEM) was performed in CH_3CN and MeOH solvents (Fig. S1). Irrespective of the solvent chosen, the compound forms a long helical fibril morphology, which indicates that compound **1c** exhibits strong aggregation due to the formation of intermolecular H-bonding (Fig. 2A, S1A and C). On the contrary, compound **1c′** did not form any long helical fibril morphology in either CH_3CN or MeOH solvent (Fig. S1B and D). In MeOH solvent, **1c′** formed small spherical structures with an average diameter of 0.39 μm. In the case of the CH_3CN solvent, an insignificant assembly of the compound was noticed (Fig. 2B). This data indicated that even though compound **1c** formed a strong aggregation, the corresponding protransporter **1c′** did not show any strong aggregation property.

2.3 Ion binding studies

The ion binding efficiencies of active transporter **1c** and protransporter **1c′** were investigated by ^1H NMR titration in acetonitrile-d_3 with a host concentration of 2 mM.[22] An increase in the equivalent of the tetrabutylammonium chloride (TBACl) salt
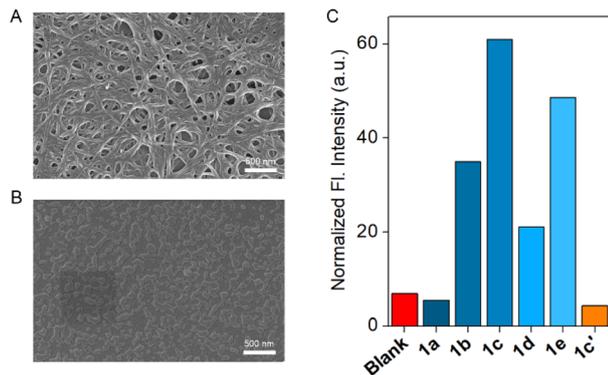
Fig. 2 Morphological study of **1c** (A) and **1c′** (B) in CH$_3$CN solvent by using FESEM. Ion transport activity comparison of **1a–1e** and **1c′** across EYPC-LUVs ⊃ HPTS (C).

with compound **1c** showed a significant downfield shift of the H$_a$, H$_b$, and H$_c$ protons (Fig. S4), confirming the involvement of these protons in the overall ion binding process through the N–H···Cl$^-$ and two aromatic C–H···Cl$^-$ hydrogen bonding interactions. Whereas, an insignificant downfield shift of compound **1c′** was noticed upon the addition of the TBACl salt (Fig. S13), confirming that compound **1c′** is inefficient in binding the Cl$^-$ ion in the ion binding pocket. A significant change in the peak position during the titration with compound **1c** and TBACl salt inspired us to investigate the ion binding process with the other TBAX (X$^-$ = Br$^-$, I$^-$, NO$_3^-$, and ClO$_4^-$) salts (Fig. S6–S12). Titration data indicated that increasing the size of the anion decreases the downfield shift of the H$_a$, H$_b$, and H$_c$ protons. In the case of TBAClO$_4$, an insignificant change in the peak position was noticed, indicating that the larger size of the ClO$_4^-$ ion restricts it from binding in the ion binding pocket of compound **1c**. The BindFit v0.5 program[23] was further used to investigate the binding constant of compound **1c** with TBAX salt. A 1 : 1 model of host:guest confirmed that compound **1c** has the highest ion binding constant for Cl$^-$ ion (26 055 M^{-1} ± 35%) followed by the Br$^-$ (2301 M^{-1} ± 9%), NO$_3^-$ (91 M^{-1} ± 1%), and I$^-$ (79 M^{-1} ± 2%) ions. An insignificant change in the peak positions during the titration of compound **1c** with TBAClO$_4$ and **1c′** with TBACl restricts us from investigating the corresponding ion binding constant. The efficiency of the Cl$^-$ ion binding was also confirmed with HRMS spectra (Fig. S14).[24] An equimolar mixing of **1c** and TBACl provided the mass corresponding to the [**1c** + Cl$^-$] complex, reconfirming the formation of 1 : 1 host : guest complex.

2.4 Transmembrane ion transport

A significant change in the ion binding constant of compound **1c** with different TBAX salts led us to check its ion transport ability across the vesicular membrane. An egg yolk phosphatidylcholine large unilamellar vesicles (EYPC-LUVs), entrapped with a pH-sensitive 8-hydroxypyrene-1,3,6-trisulfonate (HPTS, pK_a = 7.2) dye,[25–27] was used for evaluation of an initial assessment of the ion transport activity of compounds **1a–1e** and **1c′**. During the investigation of the transport studies, a 0.8 unit of

pH gradient (pH$_{in}$ = 7 and pH$_{out}$ = 7.8) was created by the exogenous addition of 20 μL of the 0.5 M NaOH solution at t = 20 s. Then, the change in the HPTS fluorescence activity was monitored over time after the addition of the transporters at t = 100 s. Finally, Triton X-100 was added at t = 300 s to lyze the vesicles to achieve maximum fluorescence intensity of the HPTS dye. An initial transport activity screening of the compounds **1a–1e** and **1c′** at 100 nM concentration showed a significant variation of the transport activity upon changing the substitution. Comparison data showed the activity sequence **1c** > **1e** > **1b** > **1d** > **1a** ≈ **1c′** (Fig. 2C and S16). The marked difference between compound **1c** and its corresponding protransporter **1c′** suggests the potential for their application as an OFF-to-ON transport system activated by specific stimuli. Further, a concentration-dependent ion transport activity was investigated for compounds **1b–1e** (Fig. S17–S20). The insufficient transport activity of the **1a** and **1c′** restricts us from investigating their concentration-dependent study. A Hill analysis of compounds **1b–1e** validated that compound **1c** has the lowest EC$_{50}$ value (109.63 ± 9.92 nM, 0.16 mol%), followed by compounds **1e** (188.96 ± 82.95 nM, 0.28 mol%), **1b** (0.93 ± 0.1 μM, 1.38 mol%), and **1d** (1.90 ± 2.99 μM, 2.81 mol%). This sequence also supported the earlier-mentioned activity comparison. The EC$_{50}$ value of compounds **1a** and **1c′** cannot be evaluated due to their insignificant transport activity. Analysis of all compounds revealed a Hill coefficient (n) ≈ 1, indicating the formation of a thermodynamically stable self-assembled ion channel across the bilayer membrane.

2.5 Ion selectivity studies

To investigate the ion selectivity of the designed compound, the most transport-active compound, **1c**, was used. To elucidate the involvement of different ions in the transport process, firstly, the anion selectivity of compound **1c** was investigated across the EYPC-LUVs ⊃ HPTS by changing the extravesicular NaX (X$^-$ = Cl$^-$, Br$^-$, I$^-$, NO$_3^-$, and OAc$^-$) salts.[28,29] A prominent variation in the ion transport activity confirmed the involvement of the anions in the overall transport process. The observed anion selectivity order is Cl$^-$ > OAc$^-$ ≈ I$^-$ > Br$^-$ > NO$_3^-$ (Fig. 3B). The experimentally obtained results did not follow any of the
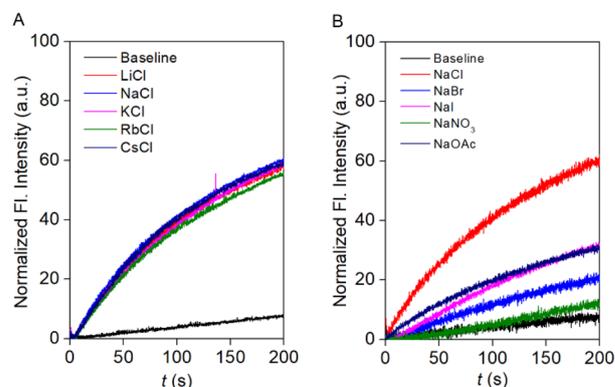

Fig. 3 Cation (A) and anion (B) selectivity of compound **1c** across EYPC-LUVs ⊃ HPTS at 100 nM concentration.

Hofmeister series, indicating that a combination of hydration energy and size of the anions governs anion selectivity (Fig. S21). To address the involvement of the cations in the ion transport process, the extravesicular MCl salts (M$^+$ = Li$^+$, Na$^+$, K$^+$, Rb$^+$, and Cs$^+$) were varied. An insignificant change in the ion transport activity was noticed during the alteration of the extravesicular cations (Fig. 3A). These data validated that cations are not involved in the overall transport process.

2.6 Chloride influx and cation selectivity studies

For assurance of the capability of the Cl$^-$ ion transport by compound **1c**, a halide-sensitive lucigenin dye was used.[30,31] During the experiment, EYPC-LUVs were entrapped with 1 mM lucigenin and 200 mM NaNO$_3$ at pH 7.0. The change in the lucigenin fluorescence activity was monitored in the presence of the compound **1c** by creating a Cl$^-$/NO$_3^-$ gradient. As expected, increasing the concentration of compound **1c** increases the lucigenin fluorescence quenching (Fig. S23), indicating that compound **1c** is capable of translocating the Cl$^-$ ion across the membrane.

Furthermore, the involvement of cation selectivity was verified across the EYPC-LUVs system using lucigenin by varying the extravesicular MCl salt (M$^+$ = Li$^+$, Na$^+$, K$^+$, Rb$^+$, and Cs$^+$). As expected, an indistinguishable change in the lucigenin fluorescence activity was noticed (Fig. S24), confirming that compound **1c** cannot transport the cations across the membrane. This cation selectivity also supports our earlier observation during the cation selectivity assay across the EYPC-LUVs ⊃ HPTS.

2.7 Mechanistic studies

A prominent selectivity towards anions makes it crucial to understand the transport mechanism operated by compound **1c**. Antiport (OH$^-$/A$^-$ or H$^+$/M$^+$, where A$^-$ and M$^+$ are anions and cations) or symport (M$^+$/OH$^-$, M$^+$/A$^-$ or H$^+$/A$^-$) of the ions can cause an increment in the HPTS fluorescence activity. The non-involvement of the metal ions rules out the possibility of symport of M$^+$/OH$^-$, M$^+$/A$^-$ ions, and antiport of H$^+$/M$^+$. Initially, the change in the Cl$^-$ influx by compound **1c** was monitored in the absence and presence of valinomycin (a K$^+$ ion transporter).[32] If compound **1c** transports the ions *via* an antiport mechanism, it is expected to couple with the valinomycin and enhance the influx of the Cl$^-$ ions in the presence of the valinomycin. On the contrary, in the case of the symport process, the Cl$^-$ influx process is expected to remain unaltered in the presence of valinomycin. Interestingly, a significant enhancement in the lucigenin fluorescence quenching was observed in the presence of valinomycin (Fig. S26). This data preliminarily indicated that compound **1c** follows the antiport as a dominant transport mechanism. Moreover, to confirm the transport mechanism, a NO$_3^-$/SO$_4^{2-}$ assay was carried out.[33] During the assay, the EYPC-LUVs were entrapped with 1 mM lucigenin and 200 mM NaCl, and the pH was adjusted to 7.0. An extravesicular solution of iso-osmolar NaNO$_3$ or Na$_2$SO$_4$ was used to create the ionic gradient, and fluorescence intensity was monitored after the addition of compound **1c**. SO$_4^{2-}$ is a do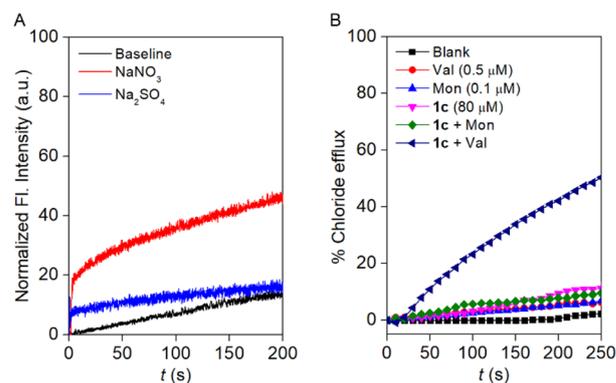ubly negatively charged anion and, thereby, difficult to transport across the bilayer compared to the NO$_3^-$ ion. It is expected that if compound **1c** follows the antiport process as the transport mechanism, then changing the extravesicular ion from NO$_3^-$ to SO$_4^{2-}$ will significantly reduce the fluorescence activity gain of the lucigenin dye. Notably, a significant difference in the fluorescence activity of the lucigenin dye was noticed upon variation of the extravesicular NaNO$_3$ salt to Na$_2$SO$_4$ salt (Fig. 4A). This data confirmed that compound **1c** predominantly follows the antiport as a transport mechanism.

Fig. 4 Cl$^-$ efflux by compound **1c**′ (2.5 μM) across EYPC-LUVs ⊃ lucigenin with intravesicular NaCl salt and iso-osmolar NaNO$_3$ or Na$_2$SO$_4$ as extravesicular salt (A). Cl$^-$ ion efflux by **1c** in the absence and presence of monensin and valinomycin (B).

Additionally, an ion-selective electrode (ISE) assay was conducted in the presence of valinomycin (an electrogenic K$^+$ carrier) and monensin (an electroneutral H$^+$/K$^+$ antiporter) to unveil the ion transport mechanism. An insignificant enhancement in the Cl$^-$ ion efflux was observed in the presence of monensin, confirming that electroneutral transport is not occurring by compound **1c**. Whereas a significant enhancement in the Cl$^-$ ion efflux was noticed in the presence of valinomycin, divulging that compound **1c** followed mainly the electrogenic mode of ion transport (Fig. 4B). Subsequently, the effect of compound **1c** on the membrane was investigated by 5(6)-carboxyfluorescein (CF) assay.[34] CF is a self-quenching dye; therefore, the encapsulation of 50 mM of CF dye across the EYPC-LUVs quenches the fluorescence activity of the CF dye. In case of CF dye leakage, the fluorescent activity is expected to be enhanced due to the decrease in the concentration of the CF dye in the bulk solution. Interestingly, no significant enhancement in the CF fluorescence activity was observed upon the addition of compound **1c** at different concentrations (Fig. S29). This data validated that compound **1c** cannot form any pores across the membrane or disintegrate the bilayer membrane.

2.8 Mode of ion transport

The transport of ions can occur either through the carrier or channel mode across the membrane. Initially, a DPPC-based assay was conducted to understand the mode of the transport process.[35,36] DPPC has a phase transition temperature of 41 °C. Hence, if the transporter behaves as a carrier, the corresponding ion transport activity is expected to decrease below 41 °C due to the difficulty in the shuttling movement of the carrier. Whereas,

in the case of the channel, irrespective of whether it is above or below the transition temperature of the DPPC lipid, the transport activity is expected to show an insignificant change or remain unaltered. During the experiment, regardless of the temperature, no discernible change in transport activity was observed (Fig. S30). This data rules out the possibility of the carrier mechanism and provides preliminary support for channel formation by compound **1c** in the membrane.

Finally, the real-time channel formation by the compound **1c** was investigated across the black lipid membrane (BLM).[33] A bilayer membrane was formed by painting a solution of di-phytanoyl phosphatidylcholine (diPhyPC) lipid in *n*-decane across the orifice of a polystyrene chamber. Both the *cis* and *trans* chambers were filled with an unbuffered 1 M KCl solution. The addition of the **1c** (5 μM) in the *cis* chamber rapidly turns on the opening-closing events at +ve and −ve holding potentials. This data confirmed that compound **1c** is capable of forming an ion channel in the membrane with an average diameter of 4.7 ± 0.3 Å. Further, the single-channel conductance of compound **1c** was investigated with a symmetric 1 M unbuffered KCl solution (Fig. 5B and S32). A distinct linear increment in the current was noticed with an increase in the voltage. This data indicated that our developed channel obeyed the ohmic behavior and is non-dipolic. The average single channel conductance with compound **1c** was 165 ± 1 pS.

Further, the anion/cation selectivity was determined using *cis/trans* = 1 M/2 M KCl salt. A distinct −ve reversible voltage was noticed with an average reversible voltage (V_r) of −6.95 mV (Fig. 5C and S33). The reversible voltage was used further to evaluate the permeability ratio. The experimentally evaluated average permeability ratio $P_{Cl^-}/P_{K^+} = 5.0 ± 1.3$, confirming that

1c exhibits 5 times higher permeability towards the Cl⁻ ion compared to the K⁺ ion.

2.9 GSH-triggered activation of ion transport

Before evaluating the GSH-based transport activation process, the efficient release of the active transporter **1c** from the pro-transporter **1c'** was evaluated by the ¹H NMR experiment. A 2 mM stock solution of compound **1c'** was prepared in the DMSO-d_6 solvent in an NMR tube. The generation of the **1c** was monitored by sequential addition of the GSH into the NMR tube. An instantaneous change in the peak positions of the $H_a' \rightarrow H_a$, $H_b' \rightarrow H_b$, $H_c' \rightarrow H_c$, and $H_d' \rightarrow H_d$ was noticed after the addition of 2 equivalents of GSH in the NMR tube (Fig. S34). This data indicated the successful conversion of the pro-transporter **1c'** to the active transporter **1c** upon the addition of the GSH. Further HRMS was collected after reacting compound **1c'** with GSH to understand the successful formation of the side product GS-DNB. A distinct peak in the HRMS spectra verified the successful formation of the GS-DNB (Fig. S35) during the generation of **1c** from **1c'**. Although the cleavage of DNB is known to be more pronounced in the presence of GSH,[21] we have also tested the cleavage of the DNB group using $Na_2S_2O_4$ as a reducing agent. We observed insignificant changes in the ¹H NMR spectrum after the addition of 2 equivalents of $Na_2S_2O_4$ (Fig. S37), indicating that the cleavage of the DNB group is not susceptible to $Na_2S_2O_4$.

Finally, GSH-based channel activation was carried out across the black lipid membrane (BLM). The addition of pro-transporter **1c'** showed no opening-closing events even after the addition of 2–3 h, indicating that inadequate self-assembly restricts it from forming a stable ion channel in the membrane. Whereas the addition of the 3 equivalents of GSH rapidly triggered the frequent opening-closing events at different holding potentials (Fig. 5A). The frequent opening-closing events are due to the *in situ* release of channel-forming compound **1c** in the membrane. Therefore, this experimental data confirmed that **1c'** can be utilized as a GSH-triggered OFF-to-ON channel formation in the membrane.

2.10 Theoretical studies

Compound **1c** was crystallized by slow evaporation of MeOH solvent. The crystal structure of compound **1c** was used to understand the disassembled structure of protransporter **1c'** and find out the probable channel assembly formation by **1c** in the membrane. Initially, the monomeric unit of the crystal structure of compound **1c** was geometrically optimized with the Cl⁻ ion by using the Gaussian 09 program package[37,38] using the B3LYP functional and 6-311++G(d,p) basis set. Geometry-optimized data validated that the H_a, H_b, and H_c protons are involved in Cl⁻ ion binding (Fig. S40), corroborating the experimentally obtained ¹H NMR titration data. Based on the experimentally evaluated Hill coefficient value, a monomeric rosette of a dodecameric assembly of compound **1c** was generated by taking the monomeric layer of the crystal structure of compound **1c**. The pentyl chain was replaced with a methyl chain to reduce the computation time. Subsequently, the
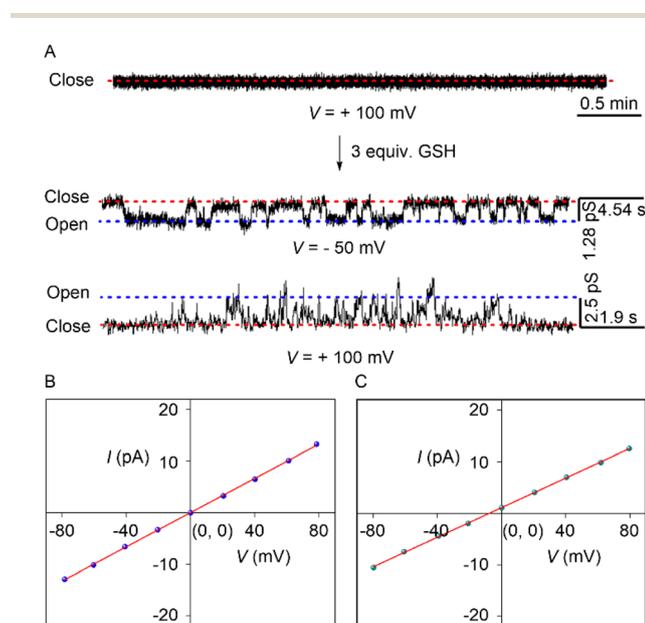

Fig. 5 Opening-closing events of *in situ* generated channel **1c** from protransporter **1c'** by GSH as stimuli (A). *I*–*V* plot of channel forming compound **1c** with symmetric (*cis/trans* = 1 M/1 M KCl) (B) and unsymmetric (*cis/trans* = 1 M/2 M KCl) (C) unbuffered KCl solution.

assembly was optimized using MOPAC software[39] with the PM6-DH+ method (Fig. 6A and S40).[40] The average calculated diameter is 3.6 ± 0.2 Å. The calculated diameter is in agreement with the experimentally evaluated channel diameter from the electrophysiological experiment. Furthermore, to understand the probable interaction of the Cl^- ion during passage through the ion translocation pathway, the Cl^- ion was placed at different positions within the monomeric rosette of the dodecameric assembly of the channel. Optimized results revealed that the Cl^- ion has hydrogen bonding interactions with the N–H and aromatic C–H protons (Fig. 6B, S41–S43). Therefore, these overall ion and channel interactions facilitate the passage of ions through the ion translocation pathway. Moreover, to understand the disassembly process of protransporter **1c′**, geometry optimization was carried out with the Gaussian 09 program package using the B3LYP functional and 6–311++G(d,p) basis set. Optimized data indicated that the 2,4-dinitrobenzene unit remains perpendicular to the isophthalamide unit (Fig. S39). Hence, the structural orientation of the molecule probably restricts it from forming a strong self-assembly *via* the formation of intermolecular H-bonding and π–π stacking interactions. This geometry optimizes data also indicated that one of the Cl^- ions of compound **1c′** preferably stays in its anion binding pocket. This data explains why compound **1c′** shows an insignificant Cl^- ion binding in the ¹H NMR titration experiment.
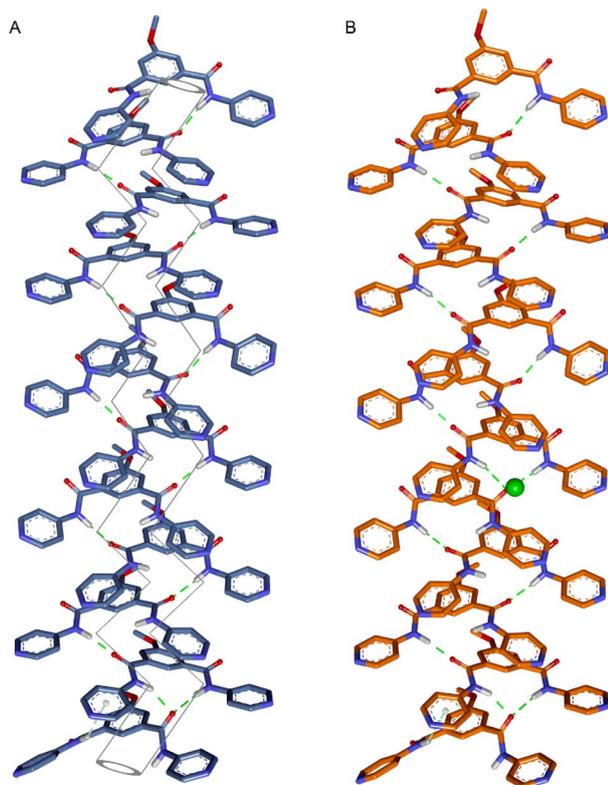

Fig. 6 Geometry optimized structure of a dodecameric assembly of the monomeric rosette of **1c** (A) and [(**1c**)$_{12}$ + Cl$^-$] (B) with an imaginary ion translocation pathway. Only polar hydrogens are shown for clarity of the structure.

3   Conclusions

We developed a glutathione (GSH)-activated synthetic anion channel system. A series of molecules was synthesized to modulate ion transport activity by varying the lipophilicity of the compounds. Among these, compound **1c** demonstrated superior ion transport efficacy. However, the corresponding protransporter **1c′** could not mediate ion transport due to inadequate self-assembly. Comprehensive transport studies revealed that compound **1c** exhibited anion selectivity, with a particular preference for Cl^- ions, and followed an antiport mechanism. Electrophysiological experiments confirmed the formation of ion channels by compound **1c** within the membrane with an average channel diameter of 4.7 ± 0.3 Å and single-channel conductance of 165 ± 1 pS. Additionally, the selectivity assay demonstrated that the ion channel exhibited five-fold greater permeability towards Cl^- ions compared to K^+ ions. A GSH-mediated activation of protransporter **1c′** initiated transport activity by releasing the channel-forming molecule **1c** within the membrane. Theoretical studies confirmed that intramolecular hydrogen bonding and π–π stacking interactions stabilize the channel assembly. Further analysis revealed that the N–H and aromatic C–H groups of the assembled channel interact with the chloride ion, and these specific channel–ion interactions cooperatively facilitate anion transport through the ion translocation pathway.

Author contributions

P. T. conceived and directed the project. S. C. carried out all of the experiments. D. G. synthesised and characterised the compounds. T. S. carried out the NMR titration experiments. S. C. and P. T. wrote the manuscript. All authors approved the final version of the manuscript.

Conflicts of interest

There are no conflicts to declare.

Data availability

CCDC 2454559 (**1c**) contains the supplementary crystallographic data for this paper.[41]

The datasets supporting this article have been uploaded as part of the supplementary information (SI). Supplementary information: data for this paper, including synthesis, compound characterization, experimental procedures, and theoretical calculations. See DOI: https://doi.org/10.1039/d6sc00359a.

Acknowledgements

Notes and references

1 C. Duran, C. H. Thompson, Q. Xiao and H. C. Hartzell, *Annu. Rev. Physiol.*, 2010, **72**, 95–121.

2 T. J. Jentsch, V. Stein, F. Weinreich and A. A. Zdebik, *Physiol. Rev.*, 2002, **82**, 503–568.

3 D. C. Gadsby, *Nat. Rev. Mol. Cell Biol.*, 2009, **10**, 344–352.

4 G. Bernard and M. I. Shevell, *Pediatr. Neurol.*, 2008, **38**, 73–85.

5 J. Y. Choi, D. Muallem, K. Kiselyov, M. G. Lee, P. J. Thomas and S. Muallem, *Nature*, 2001, **410**, 94–97.

6 T. J. Jentsch, T. Maritzen and A. A. Zdebik, *J. Clin. Invest.*, 2005, **115**, 2039–2046.

7 E. N. W. Howe, N. Busschaert, X. Wu, S. N. Berry, J. Ho, M. E. Light, D. D. Czech, H. A. Klein, J. A. Kitchen and P. A. Gale, *J. Am. Chem. Soc.*, 2016, **138**, 8301–8308.

8 Y. R. Choi, B. Lee, J. Park, W. Namkung and K.-S. Jeong, *J. Am. Chem. Soc.*, 2016, **138**, 15319–15322.

9 S. V. Shinde and P. Talukdar, *Angew. Chem., Int. Ed.*, 2017, **56**, 4238–4242.

10 J.-Y. Chen and J.-L. Hou, *Org. Chem. Front.*, 2018, **5**, 1728–1736.

11 A. Docker, T. G. Johnson, H. Kuhn, Z. Zhang and M. J. Langton, *J. Am. Chem. Soc.*, 2023, **145**, 2661–2668.

12 J. A. Malla, R. M. Umesh, S. Yousf, S. Mane, S. Sharma, M. Lahiri and P. Talukdar, *Angew. Chem., Int. Ed.*, 2020, **59**, 7944–7952.

13 P. Talukdar, G. Bollot, J. Mareda, N. Sakai and S. Matile, *Chem.–Eur. J.*, 2005, **11**, 6525–6532.

14 B. Zhou and F. P. Gabbaï, *Chem. Sci.*, 2020, **11**, 7495–7500.

15 J. A. Malla, V. K. Sharma, M. Lahiri and P. Talukdar, *Chem.–Eur. J.*, 2020, **26**, 11946–11949.

16 S. Chattopadhayay, P. Wanjari and P. Talukdar, *Chem. Sci.*, 2024, **15**, 17017–17025.

17 S. Chattopadhayay, K. V Banzal and P. Talukdar, *Angew. Chem., Int. Ed.*, 2025, **64**, e202414354.

18 N. Akhtar, N. Pradhan, A. Saha, V. Kumar, O. Biswas, S. Dey, M. Shah, S. Kumar and D. Manna, *Chem. Commun.*, 2019, **55**, 8482–8485.

19 M. Fares, X. Wu, D. Ramesh, W. Lewis, P. A. Keller, E. N. W. Howe, R. Pérez-Tomás and P. A. Gale, *Angew. Chem., Int. Ed.*, 2020, **59**, 17614–17621.

20 S. Srimayee, S. R. Badajena, N. Akhtar, M. K. Kar, S. Dey, P. Mohapatra and D. Manna, *Chem. Commun.*, 2023, **59**, 12759–12762.

21 C. Zhan, G. Zhang and D. Zhang, *ACS Appl. Mater. Interfaces Mater.*, 2018, **10**, 12141–12149.

22 W.-L. Huang, X.-D. Wang, Y.-F. Ao, Q.-Q. Wang and D.-X. Wang, *J. Am. Chem. Soc.*, 2020, **142**, 13273–13277.

23 *BindFit v0.5*, http://app.supramolecular.org/bindfit/.

24 T. Saha, S. Dasari, D. Tewari, A. Prathap, K. M. Sureshan, A. K. Bera, A. Mukherjee and P. Talukdar, *J. Am. Chem. Soc.*, 2014, **136**, 14128–14135.

25 K. Kano and J. H. Fendler, *Biochim. Biophys. Acta*, 1978, **509**, 289–299.

26 N. R. Clement and J. M. Gould, *Biochemistry*, 1981, **20**, 1534–1538.

27 H. Behera and N. Madhavan, *J. Am. Chem. Soc.*, 2017, **139**, 12919–12922.

28 A. Roy, D. Saha, A. Mukherjee and P. Talukdar, *Org. Lett.*, 2016, **18**, 5864–5867.

29 A. Roy, A. Gautam, J. A. Malla, S. Sarkar, A. Mukherjee and P. Talukdar, *Chem. Commun.*, 2018, **54**, 2024–2027.

30 H. Valkenier, C. M. Dias, K. L. P. Goff, O. Jurček, R. Puttreddy, K. Rissanen and A. P. Davis, *Chem. Commun.*, 2015, **51**, 14235–14238.

31 M. Chvojka, A. Singh, A. Cataldo, A. Torres-Huerta, M. Konopka, V. Šindelář and H. Valkenier, *Analysis Sensing*, 2024, **4**, e202300044.

32 S. V. Shinde and P. Talukdar, *Angew. Chem., Int. Ed.*, 2017, **56**, 4238–4242.

33 S. Chattopadhayay, A. Ghosh, T. K. Mukhopadhyay, R. Sharma, A. Datta and P. Talukdar, *Angew. Chem., Int. Ed.*, 2023, **62**, e202313712.

34 J. N. Weinstein, R. D. Klausner, T. Innerarity, E. Ralston and R. Blumenthal, *Biochim. Biophys. Acta*, 1981, **647**, 270–284.

35 S. Kar and N. Madhavan, *Chem.–Eur. J.*, 2023, **29**, e202301020.

36 A. Fuertes, M. Amorín and J. R. Granja, *Chem. Commun.*, 2020, **56**, 46–49.

37 M. J. Frisch, J. A. Pople and J. S. Binkley, *J. Chem. Phys.*, 1984, **80**, 3265–3269.

38 M. J. Frisch, G. W. Trucks, H. B. Schlegel, G. E. Scuseria, M. A. Robb, J. R. Cheeseman, G. Scalmani, V. Barone, B. Mennucci, G. A. Petersson, H. Nakatsuji, M. Caricato, X. Li, H. P. Hratchian, A. F. Izmaylov, J. Bloino, G. Zheng, J. L. Sonnenberg, M. Hada, M. Ehara, K. Toyota, R. Fukuda, J. Hasegawa, M. Ishida, T. Nakajima, Y. Honda, O. Kitao, H. Nakai, T. Vreven, J. A. Montgomery Jr, J. E. Peralta, F. Ogliaro, M. Bearpark, J. J. Heyd, E. Brothers, K. N. Kudin, V. N. Staroverov, T. Keith, R. Kobayashi, J. Normand, K. Raghavachari, A. Rendell, J. C. Burant, S. S. Iyengar, J. Tomasi, M. Cossi, N. Rega, J. M. Millam, M. Klene, J. E. Knox, J. B. Cross, V. Bakken, C. Adamo, J. Jaramillo, R. Gomperts, R. E. Stratmann, O. Yazyev, A. J. Austin, R. Cammi, C. Pomelli, J. W. Ochterski, R. L. Martin, K. Morokuma, V. G. Zakrzewski, G. A. Voth, P. Salvador, J. J. Dannenberg, S. Dapprich, A. D. Daniels, O. Farkas, J. B. Foresman, J. V. Ortiz, J. Cioslowski and D. J. Fox, *Gaussian 09, Rev. D.01*, Gaussian, Inc., Wallingford, CT, 2013.

39 J. J. P. Stewart, *MOPAC2012; Stewart Computational Chemistry: Colorado Springs*, CO, 2012, http://openmopac.net/.

40 M. Korth, *J. Chem. Theory Comput.*, 2010, **6**, 3808–3816.

41 CCDC 2454559: Experimental Crystal Structure Determination, 2026, DOI: 10.5517/ccdc.csd.cc2nd5bl.